PROCEEDINGS A

royalsocietypublishing.org/journal/rspa

Research

Cite this article: Geng L, Zhang W, Zhang X, Zhou X. 2021 Topological mode switching in modulated structures with dynamic encircling of an exceptional point. *Proc. R. Soc. A* **477**: 20200766.
https://doi.org/10.1098/rspa.2020.0766

Received: 27 September 2020
Accepted: 5 January 2021

Subject Areas:
mechanical engineering, solid-state physics, structural engineering

Keywords:
exceptional point, non-Hermitian, modulated medium, chiral mode transfer, time-driven parameters

Author for correspondence:
Xiaoming Zhou
e-mail: zhxming@bit.edu.cn

[†]These authors contributed equally to this work.

Electronic supplementary material is available online at https://doi.org/10.6084/m9.figshare.c.5280495.

THE ROYAL SOCIETY PUBLISHING

Topological mode switching in modulated structures with dynamic encircling of an exceptional point

Linlin Geng[1,†], Weixuan Zhang[2,†], Xiangdong Zhang[2] and Xiaoming Zhou[1]

[1]Key Laboratory of Dynamics and Control of Flight Vehicle of Ministry of Education, School of Aerospace Engineering, and [2]Key Laboratory of Advanced Optoelectronic Quantum Architecture and Measurements of Ministry of Education, School of Physics, Beijing Institute of Technology, Beijing 100081, People's Republic of China

XZ, 0000-0002-3240-9789

Exceptional points are special degeneracies occurring in non-Hermitian systems at which both eigenfrequencies and eigenmodes coalesce simultaneously. Fascinating phenomena, including topological, non-reciprocal and chiral energy transfer between normal modes, have been envisioned in optical and photonic systems with the exceptional point dynamically encircled in the parameter space. However, it has remained an open question of whether and how topological mode switching relying on exceptional points could be achieved in mechanical systems. The present paper studies a two-mode mechanical system with an exceptional point and implements the dynamic encircling of such a point using dynamic modulation mechanisms with time-driven elasticity and viscosity. Topological mode switching with robustness against the input state and loop trajectories has been demonstrated numerically. It is found that the dynamical encircling of an exceptional point with the starting point near the symmetric phase leads to chiral mode transfer controlled mainly by the encircling direction, while non-chiral dynamics is observed for the starting point near the broken phase. Analyses also show that minor energy input is required in the process of encircling the exceptional point, demonstrating the intrinsically motivated behaviour of topological mode switching.

1. Introduction

Mode conversion with significant energy transfer among eigenmodes is one of the important features observed in dynamic mechanical systems, and its manipulation has a great potential application in the broad area of mechanical and aerospace engineering. In bulk elastic media, a longitudinal–transverse mode conversion is highly desirable for applications in ultrasonic non-destructive testing and medical diagnosis [1–3], and it can be realized under specific conditions of impinging angles and frequencies with improved conversion efficiency in artificial materials and interfaces [4–6]. In guided wave systems such as plates, the switching between symmetric and antisymmetric Lamb wave modes takes place at structural discontinuities, e.g. notches, cracks and delaminations, and can be used as a criterion for damage detection and localization [7–9]. The mode conversion can also take place between forward- and backward-propagating Lamb waves and could be used for elastic wave focusing and negative reflection [10,11]. In another example, nonlinear mode coupling among vibration modes has been demonstrated to be responsible for energy transfer from the initially excited vibrational mode to other modes [12–14] or from a directly excited structure to the nonlinear attachment [15]. This mechanism holds great potential for applications in energy harvesting [16], mass sensing [17] and noise suppression [18,19]. Recently, the topological operation around an exceptional point (EP) in non-Hermitian optical, optomechanical and microwave systems reveals an exotic capability of manipulating vibrational modes [20] and waveguide modes [21]. The EP-based mode switching depends primarily upon the intrinsic topology behaviour of the system rather than initial excitations, operation frequencies and controlling paths, while the previously mentioned schemes achieve limited success in these aspects.

The concept of an 'exceptional point' was first proposed in the perturbation theory of linear non-Hermitian operators [22]. At the EP, the eigenvalues and corresponding eigenvectors coalesce and the non-Hermitian operators become defective. In optical systems, the physics of EPs has been used to realize unidirectional invisibility [23,24], enhanced sensitivity [25,26], loss-induced transmission enhancement [27] and single-mode lasing [28]. More recently, intriguing mode-switching modulation has been reported when an EP is adiabatically and dynamically (non-adiabatically) encircled along a closed loop in the parameter space. Adiabatically encircling an EP would result in an interchange of eigenstates [29,30], which is essentially different from encircling a degeneracy in Hermitian systems where the initial and final eigenstates differ only by the Berry phase [31]. This so-called 'state-flip' property relies on the adiabatic principles, requiring an infinitely slow parametric perturbation so that the eigenstate evolution follows the adiabatic expectation, and sudden transitions between eigenstates do not occur [32,33]. However, this situation is drastically altered when an EP is encircled in a dynamical manner. In this regime, the evolutions of systematic eigenstates do not always follow the adiabatic theorem [34–36]. Instead, non-adiabatic transitions (NATs) occur, leading to a chiral behaviour, in the sense that encircling an EP in different directions would result in different final states while being irrelevant to the input states [37–39]. It has been further reported that whether or not the dynamics is chiral actually depends on the starting point/endpoint of the parametric loop [40]. For the chiral dynamics to occur, the parametric trajectory must start from a point where the two eigenmodes share nearly the same gain and loss [41,42]. These theoretical findings have been demonstrated experimentally in an optomechanical system [20] and optical waveguide system [40,42,43]. Acoustic EPs have also been observed in synthetic media [44,45] or coupled structures [46,47], and they are used to realize invisible acoustic sensing [48], unidirectional near-zero reflection and focusing [49–51] and perfect absorption [52,53]. In a mechanical system, a non-Hermitian PT-symmetric beam based on shunted piezoelectric patches was proposed, where EPs were identified at the unidirectional reflectionlessness points [54,55]. The periodic laminates with the EP exhibited negative refraction, beam steering and splitting [56]. However, little attention has been focused on the dynamical modulations around an EP. Until now, an in-depth understanding of the EP phenomenon in mechanical systems, especially that of the eigenmode evolution in the process of dynamically encircling the EP, has been lacking. How can we temporally modulate the

royalsocietypublishing.org/journal/rspa Proc. R. Soc. A 477: 20200766

mechanical system to evolve along a closed parametric path that encloses an EP? Would the same mode-switching behaviour persist if an EP is dynamically encircled in mechanical systems? These open questions are yet to be explored.

In this work, we investigate mode-switching manipulation in a two-mode mass–spring–dashpot mechanical system by implementing dynamic modulations around an EP. The structure of the paper is as follows. In §2, we first show the topological configuration of system eigenvalues in the parameter space. Then, to implement the dynamical encircling of an EP in the parameter space, a modulated structure with effective time-varying elasticity and viscosity is proposed. Different scenarios of the loops enclosing the EP are illustrated. In §3, numerical simulations are performed to analyse the eigenmode evolution along with parametric loops with the starting point/endpoint lying near the symmetric phase. The chiral mode switching is observed and demonstrated to be robust against shape variations in the control paths. When the starting point/endpoint moves to the broken phase, the state evolutions exhibit non-chiral dynamics, as will be discussed in §4. Concluding remarks are outlined in §5.

2. Theoretical formulation of structural dynamics in the coupled resonator system

(a) Exceptional point in a coupled resonator

Consider two sets of mass–spring–dashpot resonators coupled by an elastic spring of k_0, as depicted in figure 1, where the weight of the mass, spring constant and damping coefficient in each element are denoted by m_i, k_i and c_i ($i = 1, 2$), respectively. The dimensionless equations of the motion for each of the masses can be expressed as

$$\begin{cases} \dfrac{\mathrm{d}^2 u_1}{\mathrm{d}\tau^2} + \xi_1 \dfrac{\mathrm{d}u_1}{\mathrm{d}\tau} = -u_1 - \kappa_0(u_1 - u_2), \\ \delta \dfrac{\mathrm{d}^2 u_2}{\mathrm{d}\tau^2} + \xi_2 \dfrac{\mathrm{d}u_2}{\mathrm{d}\tau} = -\kappa_2 u_2 + \kappa_0(u_1 - u_2), \end{cases} \tag{2.1}$$

where $u_i(\tau)$ denotes the displacement of the mass m_i at time $\tau = \omega_1 t$ with $\omega_1 = \sqrt{k_1/m_1}$, and the normalized parameters $\kappa_0 = k_0/k_1$, $\kappa_2 = k_2/k_1$, $\xi_1 = c_1/(m_1\omega_1)$, $\xi_2 = c_2/(m_1\omega_1)$, $\delta = m_2/m_1$ have been used. By introducing the state vector $\mathbf{z} = [u_1, u_2, \mathrm{d}u_1/\mathrm{d}\tau, \mathrm{d}u_2/d\tau]^T$, the equation of motion (2.1) can be further expressed as

$$\mathbf{A}\frac{\mathrm{d}}{\mathrm{d}\tau}\mathbf{z} + \mathbf{B}\mathbf{z} = 0, \tag{2.2}$$

where the 4×4 matrices $\mathbf{A}$ and $\mathbf{B}$ are given by

$$\mathbf{A} = \begin{bmatrix} \mathbf{C} & \mathbf{M} \\ \mathbf{M} & \mathbf{0} \end{bmatrix}, \quad \mathbf{B} = \begin{bmatrix} \mathbf{K} & \mathbf{0} \\ \mathbf{0} & -\mathbf{M} \end{bmatrix}, \tag{2.3}$$

with

$$\mathbf{M} = \begin{bmatrix} 1 & 0 \\ 0 & \delta \end{bmatrix}, \mathbf{C} = \begin{bmatrix} \xi_1 & 0 \\ 0 & \xi_2 \end{bmatrix}, \mathbf{K} = \begin{bmatrix} 1 + \kappa_0 & -\kappa_0 \\ -\kappa_0 & \kappa_2 + \kappa_0 \end{bmatrix}. \tag{2.4}$$

Assuming harmonic solutions of the form $\mathbf{z} = \mathbf{Z}e^{\lambda\tau}$ with $\mathbf{Z} = [\mathrm{u}_1, \mathrm{u}_2, \lambda\mathrm{u}_1, \lambda\mathrm{u}_2]^T$, equation (2.2) then becomes

$$\mathbf{R}\mathbf{Z} = \lambda\mathbf{Z} \quad \text{with} \mathbf{R} = -\mathbf{A}^{-1}\mathbf{B}. \tag{2.5}$$

Equation (2.5) describes a linear eigenproblem with the eigenvalue λ and eigenvector $\mathbf{Z}$. Since $\mathbf{R}$ is a real-valued matrix, $\{\lambda, \mathbf{Z}\}$ and its conjugate $\{\lambda^*, \mathbf{Z}^*\}$ are both its eigenvalues and eigenvectors. Therefore, four eigenvalue roots exist in the form of two complex conjugate pairs, here denoted by λ_1, λ_1^*, λ_2 and λ_2^*. Notice that the real parts of all eigenvalues must be negative to prevent an

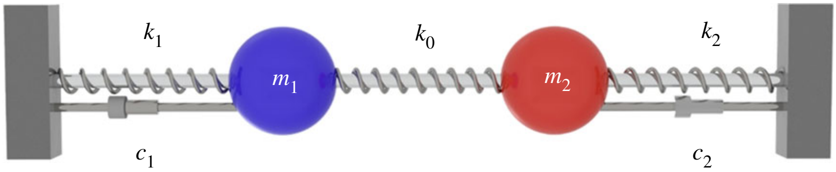

Figure 1. Schematic diagram of two sets of mass–spring–dashpot elements coupled by a linear elastic spring. (Online version in colour.)

infinite increase in state fields with time. From equation (2.5), the eigenvalue λ can be solved by

$$(\lambda^2 + \xi_1\lambda + \kappa_0 + 1)(\delta\lambda^2 + \xi_2\lambda + \kappa_0 + \kappa_2) - \kappa_0^2 = 0. \tag{2.6}$$

To develop an EP, we focus on the degeneracy of eigenvalues with $\lambda_1 = \lambda_2$. In this case, equation (2.6) should be identical in form to $(\lambda - \lambda_1)^2 (\lambda - \lambda_1^*)^2 = 0$. By equating coefficients of like terms of these two equations, we obtain the parameter conditions for the repeated eigenvalues to occur,

$$\begin{cases} 4(a_2 - \delta a_1)\delta = (\xi_2 - \delta\xi_1)(\xi_2 + \delta\xi_1), \\ \kappa_0^2(\xi_2 + \delta\xi_1)^2 = (a_2 - \delta a_1)(a_1\xi_2^2 - \delta a_2\xi_1^2), \end{cases} \tag{2.7}$$

where $a_1 = 1 + \kappa_0$ and $a_2 = \kappa_2 + \kappa_0$. The condition (2.7) would determine an EP of degeneracy in a system parameter space. Here, without loss of generality, we choose the two-dimensional (2D) parameter space (κ_2, ξ_2), and we denote the position of the EP in the parameter space by $\kappa_2 = \kappa_{EP}$ and $\xi_2 = \xi_{EP}$, which can be determined from equation (2.7).

As illustrative examples, consider values of $\kappa_0 = 0.046$, $\xi_1 = 0.01$ and $\delta = 0.684$. The coordinates of the EP can be calculated as $\kappa_{EP} \approx 0.672$ and $\xi_{EP} \approx 0.081$. We calculate the eigenvalue λ of the coupled resonator as a function of κ_2/κ_{EP} and ξ_2/ξ_{EP} and show its real and imaginary parts in figure 2*a*,*b*, respectively. The eigenvalue sheets with smaller and larger values of $|\mathrm{Re}(\lambda)|$ represent the low-loss (blue sheet) and high-loss (red sheet) eigenstates, respectively. The eigenvalue distributions in the parameter space near an EP are characterized by self-intersecting Riemann sheets. The real parts of eigenvalues coalesce in the symmetric phase line (figure 2*a*). The imaginary parts of eigenvalues are found to bifurcate (figure 2*b*), coalescing in the broken phase line and forming a branch cut (BC) near the branch point singularity (i.e. the EP). Here, the presented resonator system has shown an obvious analogy with *PT*-symmetric systems with the balanced gain and loss [40]. Therefore, we may expect the landmark effects of *PT* symmetry, such as chiral mode transmission and topological mode switching with the robustness against input states and paths, to be realized in our model when the EP is dynamically encircled.

The intriguing behaviour induced by dynamically encircling an EP is initiated in quantum systems, where two system parameters are continuously changed in time along a closed loop in parameter space around an EP. In that case, the system is described by the time-dependent Hamiltonian in the Schrödinger equation. To mimic this behaviour in mechanical systems, we temporally modulate the parameters $\kappa_2(\tau)$ and $\xi_2(\tau)$ to encircle the EP in the parameter space (κ_2, ξ_2). However, a time change in mechanical properties of materials is not easily realized and controlled. To achieve this goal, the concept of dynamic mechanism metamaterials will be used, which has proven to be a new and effective approach to acquiring periodically time-varying material properties [57,58]. The dynamic mechanism metamaterials consist of the spinning elements with time periodicity. This feature properly fulfils the requirement of encircling the EP with easy tuning of the starting point, the loop's encircling direction and the trajectory, as we will discuss in the following sections.

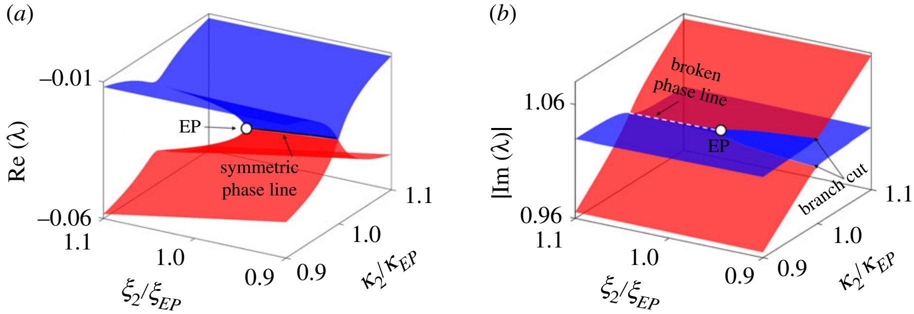

Figure 2. Patterns of (*a*) real and (*b*) imaginary parts of eigenvalues in the two-dimensional parameter space (κ_2, ξ_2). (Online version in colour.)

(b) A modulated structure with time-varying stiffness and viscosity

The time-modulated structure capable of the dynamic encircling of an EP is designed as shown in figure 3. Based on the prior model shown in figure 1, we connect the mass m_2 to the spring and dashpot mechanisms that rotate with the spinning axis vertical to the main track. Notice that the dashpot c_4 rotates with a constant angular frequency Ω_r from the initial biasing angle ψ_0, while the perpendicularly arranged springs k_4 and k_5 are allowed to undergo an arbitrary rotation $\phi(\tau)$ from the initial angle ϕ_0. Using the homogenization technique, we show that the rotating-spring and dashpot mechanisms can be effectively represented by single spring and dashpot elements with effective time-varying stiffness $\kappa_2(\tau)$ and viscosity $\xi_2(\tau)$ (see electronic supplementary material for details). The corresponding equation of motion of the modulated structure can be written as

$$\begin{cases} \dfrac{d^2u_1}{d\tau^2} + \xi_1 \dfrac{du_1}{d\tau} = -u_1 - \kappa_0(u_1 - u_2), \\ \delta \dfrac{d^2u_2}{d\tau^2} + \xi_2(\tau) \dfrac{du_2}{d\tau} = -\kappa_2(\tau) u_2 + \kappa_0(u_1 - u_2), \end{cases} \tag{2.8}$$

where effective stiffness and viscosity, $\kappa_2(\tau)$ and $\xi_2(\tau)$, are given by

$$\kappa_2(\tau) = \kappa_{\text{eff}}^0 + \kappa_{\text{eff}}^1 \cos 2\Phi(\tau), \quad \xi_2(\tau) = \xi_{\text{eff}}^0 + \xi_{\text{eff}}^1 \cos 2\Psi(\tau), \tag{2.9}$$

where $\kappa_{\text{eff}}^0 = (k_3 + k_4 + k_5)/k_1$, $\kappa_{\text{eff}}^1 = (k_4 - k_5)/k_1$, $\xi_{\text{eff}}^0 = (c_3 + c_4)/(m_1\omega_1)$ and $\xi_{\text{eff}}^1 = c_4/(m_1\omega_1)$. $\Psi(\tau) = \psi_0 \pm \omega_r \tau$ with $\omega_r = \Omega_r/\omega_1$ and $\Phi(\tau) = \phi_0 \pm \phi(\tau)$ are phase angles at instant τ, where the '+' and '−' notation represents, respectively, the anti-clockwise and clockwise rotation of dynamic modulation mechanisms. We can observe that the equation of motion (2.8) is identical in form to equation (2.1), yet additionally equipped with the time-dependent parameters $\kappa_2(\tau)$ and $\xi_2(\tau)$. This allows for the possibility of encircling the EP by the time-driven procedure in the parameter space (κ_2, ξ_2).

We now showcase the different types of loops enclosing the EP parameterized by equation (2.9). Consider the following parameters: $\kappa_{\text{eff}}^0 = 1.042\kappa_{EP}$, $\kappa_{\text{eff}}^1 = 0.268\kappa_{EP}$,$\xi_{\text{eff}}^0 = 0.741\xi_{EP}$, $\xi_{\text{eff}}^1 = 0.617\xi_{EP}$ and $\omega_r = 0.06$. An elliptic loop, the simplest case realized by the model, is formed when the spring mechanism rotates with the phase angle varying linearly in time $\phi(\tau) = \omega_r\tau$. By choosing the initial state $\phi_0 = 3\pi/4$ and $\psi_0 = \pi/2$ and the spinning direction '+' for dynamic mechanisms such that $\Phi(\tau) = 3\pi/4 + \omega_r\tau$ and $\Psi(\tau) = \pi/2 + \omega_r\tau$, we can realize the anti-clockwise loop with the starting point near the symmetric phase of the Riemann sheets (figure 4*a*). The time-driven parameter point (κ_2,ξ_2) returns to its starting point after enclosing the EP in time interval $0 \le \tau \le \pi/\omega_r$. If simply reversing the spinning direction from '+' to '−' for both mechanisms, we can achieve a clockwise loop with the same starting point (figure 4*b*). In another case, the anti-clockwise loop with a starting point near the broken phase of the Riemann sheets could

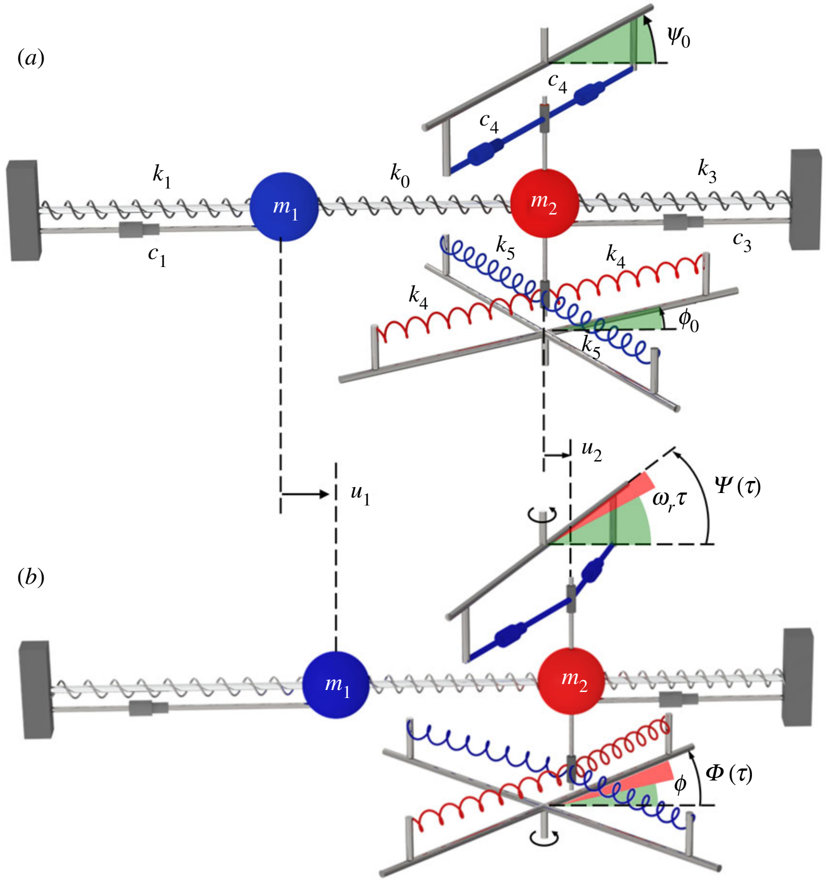

Figure 3. Schematic diagram of the modulated structure containing dynamic mechanisms. (*a*) At an initial time, the top and bottom mechanism structures form angles ψ_0 and ϕ_0 relative to the main track, respectively; (*b*) at a later time τ, the phase angles of two mechanisms are $\Psi(\tau)$ and $\Phi(\tau)$. (Online version in colour.)

be realized as shown in figure 4*c*, if we control the dynamic mechanisms with phase functions $\Phi(\tau) = \pi/4 + \omega_r\tau$ and $\Psi(\tau) = \omega_r\tau$. Finally, we show that a more complicated loop trajectory around the EP can be created if a nonlinear function $\phi(\tau) = \sin^{-1}[\sin(2\omega_r\tau)/2 + \sin(4\omega_r\tau)/6]$ is adopted. By setting phase functions $\Phi(\tau) = 3\pi/4 + \phi(\tau)$ and $\Psi(\tau) = \pi/2 + \omega_r\tau$, the anti-clockwise irregular loop with the starting point near the symmetric phase could be realized, as shown in figure 4*d*. For the rest of the paper, we shall focus on the eigenstate evolution in modulated structures for various scenarios of encircling the EP in the parameter space.

3. Dynamically encircling an exceptional point with starting points near the symmetric phase

In this section, the eigenstate evolution driven by encircling the EP will be studied for starting points near the symmetric phase. We begin by introducing the scheme for the calculation of modal amplitudes from the time domain response of modulated structures under initial conditions. Let $\boldsymbol{\psi}(\tau) = [u_1, u_2, du_1/d\tau, du_2/d\tau]^T$ denote the state vector calculated by solving equation (2.8) with specific initial conditions $\boldsymbol{\psi}(\tau = 0) = \boldsymbol{\psi}_0$. We can extract from $\boldsymbol{\psi}(\tau)$ the modal amplitudes of the instantaneous eigenstates at each time step based on the complex mode theory [59]. To apply this method, the response $\boldsymbol{\psi}$ is written in terms of instantaneous eigenstate $\mathbf{Z}_i$ and its

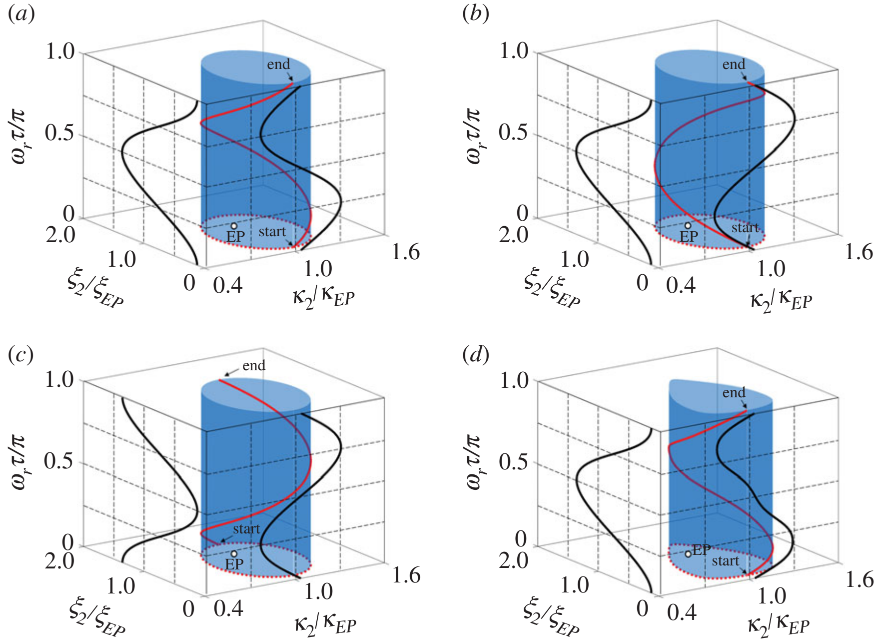

Figure 4. Different types of loops enclosing the EP parameterized by equation (2.9): (*a*) anti-clockwise and (*b*) clockwise elliptic loops with the starting point near the symmetric phase of the Riemann sheets; (*c*) anti-clockwise elliptic loop with the starting point near the broken phase; (*d*) anti-clockwise loop along the more complicated trajectory around the EP with the starting point near the symmetric phase. (Online version in colour.)

amplitude q_1 by $\boldsymbol{\psi} = q_1\mathbf{Z}_1 + q_2\mathbf{Z}_2 + q_1^*\mathbf{Z}_1^* + q_2^*\mathbf{Z}_2^*$. Multiplying $\mathbf{Z}_1^T\mathbf{A}$ on both sides of this equation gives rise to $q_1 = \mathbf{Z}_1^T\mathbf{A}\boldsymbol{\psi}/(\mathbf{Z}_1^T\mathbf{A}\mathbf{Z}_1)$, where $\mathbf{Z}_1^T\mathbf{A}\mathbf{Z}_1^* = \mathbf{Z}_1^T\mathbf{A}\mathbf{Z}_2 = \mathbf{Z}_1^T\mathbf{A}\mathbf{Z}_2^* = 0$ has been used according to the orthogonality relation [60]. Other amplitude coefficients can be determined similarly. To sum up, we can obtain that

$$q_i = \frac{\mathbf{Z}_i^T\mathbf{A}\boldsymbol{\psi}}{\mathbf{Z}_i^T\mathbf{A}\mathbf{Z}_i}, \quad q_i^* = \frac{(\mathbf{Z}_i^*)^T\mathbf{A}\boldsymbol{\psi}}{(\mathbf{Z}_i^*)^T\mathbf{A}\mathbf{Z}_i^*}. \tag{3.1}$$

The modal amplitudes are defined as $p_i = 2|q_i|$. In the following analyses, we distinguish the eigenstates by the magnitude of the real parts of the corresponding eigenvalues, i.e. $|\mathrm{Re}(\lambda)|$. Eigenstates with larger and smaller values of $|\mathrm{Re}(\lambda)|$ are termed the high-loss and low-loss modes, respectively, and we let p_H and p_L denote their modal amplitudes.

Consider phase functions $\Phi(\tau) = 3\pi/4 \pm \omega_r\tau$ and $\Psi(\tau) = \pi/2 \pm \omega_r\tau$ for the anti-clockwise or clockwise elliptic loops with the starting point near the symmetric phase, and other effective parameters of dynamic mechanics are the same as those used in figure 4. We are interested in whether the high-loss (H) or low-loss (L) mode dominates the output state for a pure H or L mode input as initial conditions. Figure 5 shows the modal amplitudes and corresponding evolution trajectories drawn on the Riemann sheets in four cases with different sets of input state and loop orientation. For the H mode input and anti-clockwise loop (figure 5*a*,*e*), the eigenstate is the first to travel on the high-loss Riemann sheet. In the beginning stage of evolution, the H state decays owing to the high loss, meanwhile the L state can become excited and its modal amplitude does not remain zero owing to non-adiabatic coupling [37,38]. Once the L state is excited, it grows and eventually overwhelms the high-loss state at a critical point, as shown by the curve crossing in figure 5*e*. In the eigenvalue spectrum (figure 5*a*), this effect is described by an abrupt drop in eigenstates from the high-loss Riemann sheet to the low-loss one; this is known as the non-adiabatic transition (NAT) [35,36]. Further evolution forces the eigenstate to go across the BC, where the two modes exchange their identity and end up with the dominant H mode ($p_\mathrm{H} > p_\mathrm{L}$).

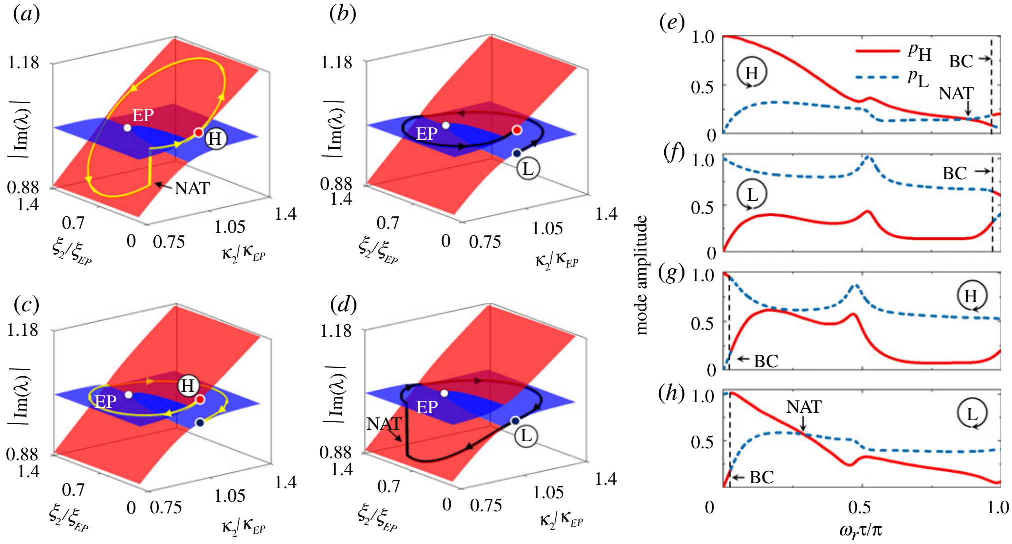

Figure 5. (*a–d*) Eigenstate evolution trajectories drawn on the Riemann sheets and (*e–h*) modal amplitudes when the EP is encircled along an elliptic loop with the starting point near the symmetric phase in four different cases of the input state and loop orientation: (*a*,*e*) the high-loss mode input and anti-clockwise orientation; (*b*,*f*) the low-loss mode input and anti-clockwise orientation; (*c*,*g*) the high-loss mode input and clockwise orientation; (*d*,*h*) the low-loss mode input and clockwise orientation. (Online version in colour.)

When the input state is the L mode (figure 5*b*,*f*), the eigenstate undergoes stable evolution on the low-loss sheet without inducing the NAT, but will be eventually transformed into the dominant H mode owing to the BC. In the clockwise loop scenario, the initial H mode is soon converted to the dominant L mode by the BC, which keeps evolving on the low-loss sheet until the end of the loop (figure 5*c*,*g*). By contrast, the input L mode, despite being switched by the BC, returns the low-loss sheet owing to the NAT (figure 5*d*,*h*). Here, we see that the output state is decided by the loop orientation—the H mode output for the anti-clockwise loop and the L mode output for the clockwise loop—regardless of the injected states. This fancy property, which solely depends on the encircling direction in the parameter space, is called 'chiral behaviour' [37].

We note from figure 5 that the NAT is characterized by the crossing of mode amplitude curves, and it takes place when the high-loss state dominates the dynamics ($p_H > p_L$), leading to the fact that the H state jumps to the low-loss Riemann sheet as required by the stability of the lossy system. In fact, the output state near the end of the loop always prefers the low-loss Riemann sheet irrespective of the input states and encircling directions. However, as long as the starting point lies near the symmetric phase where the imaginary parts of the Riemann sheets are discontinuous, the encircling direction becomes decisive for controlling the output state as a result of the deterministic mode switching by the BC. This is the key reason why the chiral dynamics appears. We stress that the chiral dynamics cannot be observed for the loop that excludes the EP. In that case, the dominant output state is always consistent with the input state (see electronic supplementary material for details).

The dynamic modulation mechanism not only provides the time-varying stiffness and viscosity, but also acts as the energy source or energy sink for the system. Below we carry out an energy analysis to quantify the magnitude of energy inputted or retracted by dynamic mechanisms in the process of encircling the EP. The net system energy E_{total} comprises the kinetic energy of the masses, the potential energy of the springs and the energy dissipated by the dashpots. The net energy input W_{input} refers to the work done by the external moment of force to acquire the desired rotation of the dynamic mechanisms. The procedure to calculate these

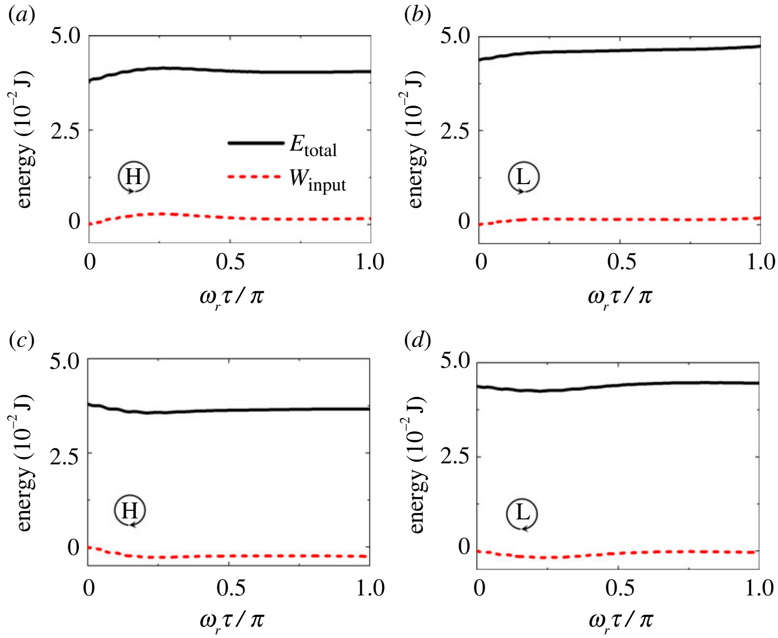

Figure 6. The system mechanical energy and net energy input in the process of encircling the EP corresponding to the four cases studied in figure 5. The parameters used are $m_1 = 100$ g, $m_2 = 68.4$ g, $k_0 = 13.8$ N m^{-1}, $k_1 = 300$ N m^{-1}, $k_3 = 60$ N m^{-1}, $k_4 = 102$ N m^{-1}, $k_5 = 48$ N m^{-1}, $c_1 = 0.055$ kg s^{-1}, $c_3 = 0.055$ kg s^{-1}, $c_4 = 0.274$ kg s^{-1}, $\Omega_r = 3.3$ rad s^{-1} and $l_0 = 15$ cm. (Online version in colour.)

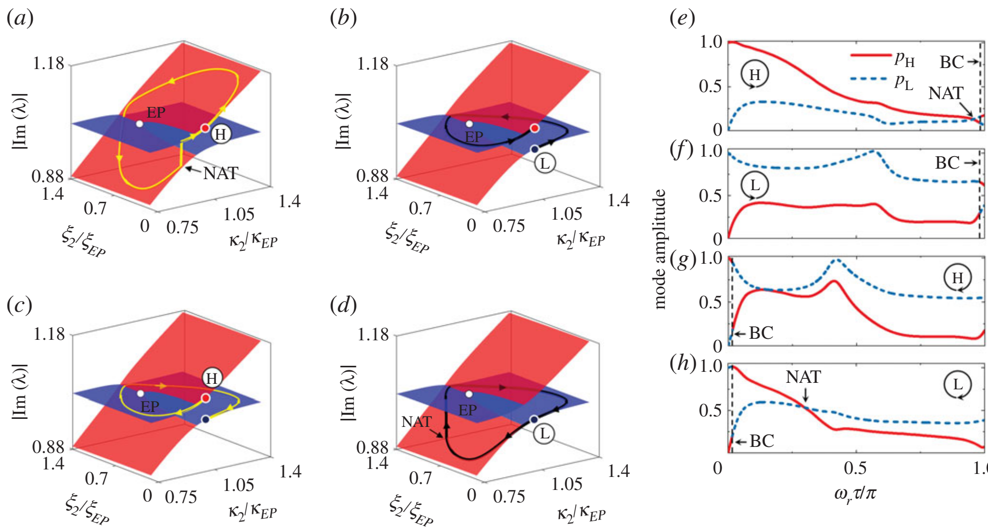

Figure 7. Results similar to those shown in figure 5, but for a parametric loop along a rather complicated trajectory instead of an elliptic loop. (Online version in colour.)

energy quantities has been provided in the electronic supplementary material. Figure 6 plots the energy E_{total} and W_{input} in the time domain for the four cases discussed in figure 5. It can be seen that the external energy input W_{input} is very small in magnitude compared with the total energy E_{total} stored in the system. Note that $W_{input} < 0$ means that energy is taken out by the dynamic mechanism. We can conclude from these results that the chiral mode switching does not

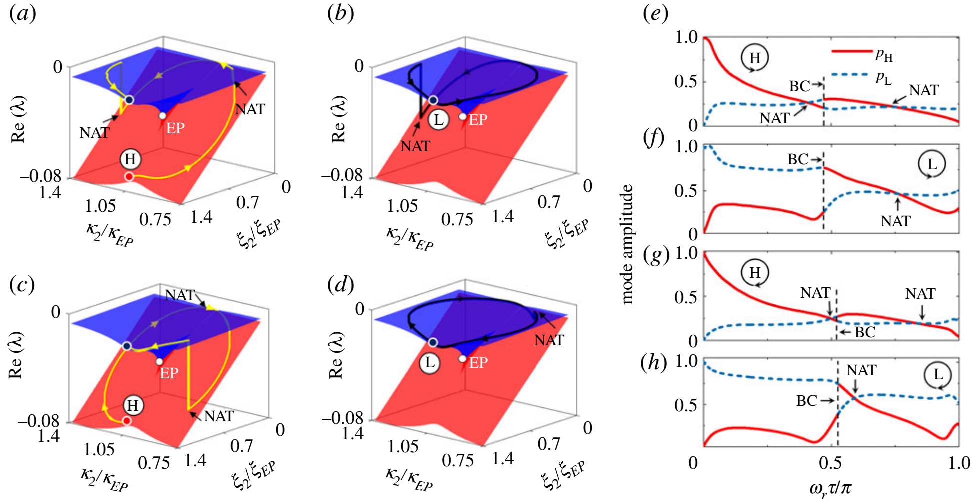

Figure 8. (*a*–*d*) Eigenstate evolution trajectories drawn on the Riemann sheets and (*e*–*h*) modal amplitudes when the EP is encircled along an elliptic loop with the starting point near the broken phase in four different cases of input state and loop orientation: (*a*,*e*) the high-loss mode input and anti-clockwise orientation; (*b*,*f*) the low-loss mode input and anti-clockwise orientation; (*c*,*g*) the high-loss mode input and clockwise orientation; (*d*,*h*) the low-loss mode input and clockwise orientation. (Online version in colour.)

stem from the energy exchanged with the surroundings, but originates from an intrinsic property associated with the special topology of the eigenvalue Riemann surface in the vicinity of the EP.

To further demonstrate that the chiral dynamics is a manifestation of the Riemann surface topology, we investigated the eigenstate evolution driven by a parametric loop along a rather complicated trajectory instead of an elliptic loop. Here, we chose the phase functions $\Phi(\tau) = 3\pi/4 \pm \phi(\tau)$ and $\Psi(\tau) = \pi/2 \pm \omega_r\tau$, where $\phi(\tau)$ is identical to that used in figure 4*d*. The results corresponding to the four cases discussed in figure 5 are analysed, showing again the chiral behaviour and the fact that the anti-clockwise (clockwise) orientation always leads to the dominant H mode (L mode), regardless of the input state (figure 7). In particular, the same fundamental features of the state evolution can be found by comparing two types of loops under identical settings of initial state and orientation. For instance, when the evolution is adiabatic without the NAT, one state can be transformed into the other owing to the BC (figure 7*b*,*f* and *c*,*g*). When the evolution is non-adiabatic, either the H or L state experiences a NAT and returns to itself at the end of the loop (figure 7*a*,*e* and *d*,*h*). This result indicates that the chiral mode switching is robust to the shape change of the loop that encloses the EP.

4. Dynamically encircling an exceptional point with starting points near the broken phase

Now we study the system response for the loop that encircles the EP from points near the broken phase. Phase functions $\Phi(\tau) = \pi/4 \pm \omega_r\tau$ and $\Psi(\tau) = \pm\omega_r\tau$, as exemplified in figure 4*c*, are chosen to calculate the time evolution of eigenstates in one loop. As illustrated in figure 2*a*, the Riemann sheets of high-loss and low-loss states are separated by a large gap in the parameter space near the broken phase. As a result, strong NATs take place for the H mode as the input state. It is evidenced from figure 8*a*,*e* and *c*,*g* that the system undergoes twice the NATs and once the BC-induced mode switching, and finally outputs the dominant L mode for both anti-clockwise and clockwise loops. When the low-loss state is inputted, both the NAT and BC occur once, and eventually the L mode returns to itself at the end of the loop (figure 8*b*,*f* and *d*,*h*). The results clearly show that the output state is always transformed into the low-loss state regardless of the input state and

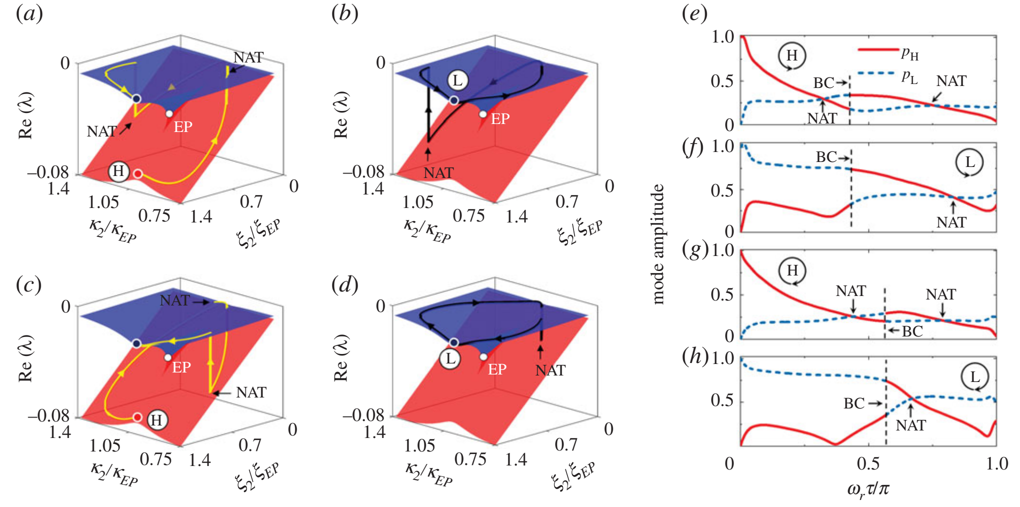

Figure 9. Results similar to those shown in figure 8, but for a parametric loop along a rather complicated trajectory instead of an elliptic loop. (Online version in colour.)

loop orientation, in distinct contrast to chiral dynamics appearing when the starting point lies near the symmetric phase. This distinction originates from the different topological structures of the eigenvalue Riemann surfaces at various regions. The orientation-independent non-chiral behaviour can be attributed to the continuous eigenvalue Riemann surface near the broken phase, whereas for the chiral dynamics the encircling loop in the parameter space should start from the point where the two eigenstates carry nearly the same real parts of the eigenvalues. Note that the non-chiral behaviour caused by the broken phase can also be observed when the EP is excluded by an elliptic loop (see electronic supplementary material for details). This phenomenon reveals the fact that the eigenstate evolution initiated from the broken phase favours the lower-loss Riemann sheet for remaining stable, regardless of whether the EP is included by the loop or not.

In the final example, we consider the complex loop trajectory described by phase functions $\Phi(\tau) = \pi/4 \pm \phi(\tau)$ and $\Psi(\tau) = \pm\omega_r\tau$; this is same as the scheme introduced in figure 4*d* except that the starting point is set close to the broken phase. The non-chiral dynamics for the eigenstate evolution can be confirmed from figure 9 by the fact that the system always outputs the low-loss state. Given the identical settings, the eigenstate along the complex trajectory evolves in exactly the same manner as the evolution operates in the elliptic loop scenario, demonstrating the robustness of the non-chiral behaviour against the shape change of the loop trajectory.

5. Conclusion

In this paper, the topological mode switching achieved by dynamically encircling an EP in a time-modulated mechanical system is studied. The modulated structure consists of two sets of mass–spring–dashpot resonators with one of them coupling to rotating-spring and rotating-dashpot dynamic mechanisms. Based on the rigorous theoretical analysis of dynamic mechanisms, we have shown that the rotary mechanisms can be effectively represented by the single-spring and dashpot elements with effective time-varying stiffness and viscosity. At any instant, the effective stiffness and viscosity constitutes a time-driven point in the parameter space, so that, when the dynamic mechanisms rotate in the prescribed manner, the system is forced to evolve along a closed parametric loop. This design scheme allows for easy control of the encircling loop in the parameter space, including control of the encircling direction, starting/end position and shape of the enclosing paths.

Based on the proposed time-modulated structure, we have demonstrated the chiral mode-switching behaviour when an EP is dynamically encircled along a parametric loop with the starting point/endpoint lying near the symmetric phase. The energy inputted or retracted by dynamic mechanisms in the EP-encircling process is also examined. It is found that the external energy input is very small in magnitude compared with the total energy stored in the system, indicating that chiral mode switching is the result of an intrinsic property associated with the dynamics of the modulated structure and is not due to energy exchange with the surroundings. When the starting point/endpoint moves to the broken phase, the non-chiral behaviour is observed, indicating that the output is always in the low-loss state regardless of the injections, encircling directions and whether the EP is encircled or not. In addition, we have proved that the chiral and non-chiral behaviours are robust against the shape changes of the loop that encloses the EP.

The fabrication feasibility of the proposed configuration is discussed finally. The proposed model is a mass–spring–damper system, which can be easily manufactured by using a rigid material, a helical spring and a dashpot with a perforated piston moving in a viscous fluid. To fabricate the dynamic modulation mechanism, a spin motor programmed to output the desired angular phase can be used to drive the rotation of the spring and dashpot elements. Thereby, it is technically feasible to fabricate the proposed configuration to meet design requirements. We note that fabrication error is inevitable and may cause a small change in the EP position in the parameter space and the shape topology of the loop that encloses the EP. However, topological mode switching by encircling the EP is insensitive to these influences, because it depends primarily on the fact that the EP is enclosed or not, while irrelevant to the specific EP position and encircling path. Therefore, the experimental demonstration of topological mode switching with a relatively high tolerance for fabrication errors can be expected. The present study is expected to open a new avenue towards mode-switching manipulation of coupled waves and vibrational modes in mechanical systems with EPs.

Data accessibility. The paper contains no experimental data. All results and illustrative computations are directly reproducible.

Authors' contributions. L.G., W.Z. and X.M.Z. conceived the core concept and mathematical model. L.G. derived the analytical results and carried out the numerical simulations. W.Z. and X.D.Z. participated in the design of the study. All authors discussed the results and commented on the manuscript. All authors approved the final version and agree to be held accountable for all aspects of the work.

Competing interests. We declare we have no competing interests.

Funding. This work was supported by the National Natural Science Foundation of China (11872111, 11991030, 11991033 and 11622215); 111 project (B16003) and the National Key R & D Program of China under grant no. 2017YFA0303800.

Acknowledgements. The authors thank Yuchen Zhao and Jiahui Huang for helpful discussions.

References

1. Clement GT, White PJ, Hynynen K. 2004 Enhanced ultrasound transmission through the human skull using shear mode conversion. *J. Acoust. Soc. Am.* **115**, 1356–1364. (doi:10.1121/1.1645610)
2. Hynynen K, McDannold N, Sheikov NA, Jolesz FA, Vykhodtseva N. 2005 Local and reversible blood–brain barrier disruption by noninvasive focused ultrasound at frequencies suitable for trans-skull sonications. *Neuroimage* **24**, 12–20. (doi:10.1016/j.neuroimage.2004.06.046)
3. Tufail Y, Yoshihiro A, Pati S, Li MM, Tyler WJ. 2011 Ultrasonic neuromodulation by brain stimulation with transcranial ultrasound. *Nat. Protoc.* **6**, 1453–1470. (doi:10.1038/nprot.2011.371)
4. Wu Y, Lai Y, Zhang Z-Q. 2011 Elastic metamaterials with simultaneously negative effective shear modulus and mass density. *Phys. Rev. Lett.* **107**, 105506. (doi:10.1103/PhysRevLett.107.105506)
5. Su X, Norris AN. 2016 Focusing, refraction, and asymmetric transmission of elastic waves in solid metamaterials with aligned parallel gaps. *J. Acoust. Soc. Am.* **139**, 3386–3394. (doi:10.1121/1.4950770)

6. Lee HJ, Lee J-R, Moon SH, Je T-J, Jeon E-C, Kim K, Kim YY. 2017 Off-centered double-slit metamaterial for elastic wave polarization anomaly. *Sci. Rep.* **7**, 15378. (doi:10.1038/s41598-017-15746-2)
7. Ramadas C, Balasubramaniam K, Joshi M, Krishnamurthy C. 2009 Interaction of the primary anti-symmetric Lamb mode (Ao) with symmetric delaminations: numerical and experimental studies. *Smart Mater. Struct.* **18**, 085011. (doi:10.1088/0964-1726/18/8/085011)
8. Okabe Y, Fujibayashi K, Shimazaki M, Soejima H, Ogisu T. 2010 Delamination detection in composite laminates using dispersion change based on mode conversion of Lamb waves. *Smart Mater. Struct.* **19**, 115013. (doi:10.1088/0964-1726/19/11/115013)
9. Ghadami A, Behzad M, Mirdamadi HR. 2015 A mode conversion-based algorithm for detecting rectangular notch parameters in plates using Lamb waves. *Arch. Appl. Mech.* **85**, 793–804. (doi:10.1007/s00419-015-0991-x)
10. Bramhavar S, Prada C, Maznev AA, Every AG, Norris TB, Murray TW. 2011 Negative refraction and focusing of elastic Lamb waves at an interface. *Phys. Rev. B* **83**, 014106. (doi:10.1103/PhysRevB.83.014106)
11. Germano M, Alippi A, Bettucci A, Mancuso G. 2012 Anomalous and negative reflection of Lamb waves in mode conversion. *Phys. Rev. B* **85**, 012102. (doi:10.1103/PhysRevB.85.012102)
12. Evan-Iwanowski RM. 1976 *Resonance oscillations in mechanical systems*. Amsterdam, The Netherlands: Elsevier.
13. Nayfeh AH, Mook DT. 1979 *Nonlinear oscillations*. New York, NY: Wiley Interscience.
14. Nayfeh AH, Balachandran B. 1989 Modal interactions in dynamical and structural systems. *Appl. Mech. Rev.* **42**, S175–S201. (doi:10.1115/1.3152389)
15. Vakakis AF, Gendelman OV, Bergman LA, McFarland DM, Kerschen G, Lee YS. 2008 *Nonlinear targeted energy transfer in mechanical and structural systems*. Dordrecht, The Netherlands: Springer.
16. Lan C, Qin W, Deng W. 2015 Energy harvesting by dynamic unstability and internal resonance for piezoelectric beam. *Appl. Phys. Lett.* **107**, 093902. (doi:10.1063/1.4930073)
17. Kirkendall CR, Howard DJ, Kwon JW. 2013 Internal resonance in quartz crystal resonator and mass detection in nonlinear regime. *Appl. Phys. Lett.* **103**, 223502. (doi:10.1063/1.4833617)
18. Kerschen G, Lee YS, Vakakis AF, McFarland DM, Bergman LA. 2005 Irreversible passive energy transfer in coupled oscillators with essential nonlinearity. *SIAM J. Appl. Math.* **66**, 648–679. (doi:10.1137/040613706)
19. Antonio D, Zanette DH, López D. 2012 Frequency stabilization in nonlinear micromechanical oscillators. *Nat. Commun.* **3**, 806. (doi:10.1038/ncomms1813)
20. Xu H, Mason D, Jiang L, Harris JGE. 2016 Topological energy transfer in an optomechanical system with exceptional points. *Nature* **537**, 80–83. (doi:10.1038/nature18604)
21. Doppler J *et al.* 2016 Dynamically encircling an exceptional point for asymmetric mode switching. *Nature* **537**, 76–79. (doi:10.1038/nature18605)
22. Kato T. 1966 *Perturbation theory for linear operators*. Berlin, Germany: Springer.
23. Lin Z, Ramezani H, Eichelkraut T, Kottos T, Cao H, Christodoulides DN. 2011 Unidirectional invisibility induced by PT-symmetric periodic structures. *Phys. Rev. Lett.* **106**, 213901. (doi:10.1103/PhysRevLett.106.213901)
24. Feng L, Xu Y-L, Fegadolli WS, Lu M-H, Oliveira JEB, Almeida VR, Chen YF, Scherer A. 2013 Experimental demonstration of a unidirectional reflectionless parity-time metamaterial at optical frequencies. *Nat. Mater.* **12**, 108–113. (doi:10.1038/nmat3495)
25. Chen W, Özdemir ŞK, Zhao G, Wiersig J, Yang L. 2017 Exceptional points enhance sensing in an optical microcavity. *Nature* **548**, 192–196. (doi:10.1038/nature23281)
26. Hodaei H, Hassan AU, Wittek S, Garcia-Gracia H, El-Ganainy R, Christodoulides DN, Khajavikhan M. 2017 Enhanced sensitivity at higher-order exceptional points. *Nature* **548**, 187–191. (doi:10.1038/nature23280)
27. Guo A, Salamo GJ, Duchesne D, Morandotti R, Volatier-Ravat M, Aimez V, Siviloglou GA, Christodoulides DN. 2009 Observation of PT-symmetry breaking in complex optical potentials. *Phys. Rev. Lett.* **103**, 093902. (doi:10.1103/PhysRevLett.103.093902)
28. Feng L, Wong ZJ, Ma R-M, Wang Y, Zhang X. 2014 Single-mode laser by parity-time symmetry breaking. *Science* **346**, 972–975. (doi:10.1126/science.1258479)
29. Dembowski C, Gräf H-D, Harney H, Heine A, Heiss W, Rehfeld H, Richter A. 2001 Experimental observation of the topological structure of exceptional points. *Phys. Rev. Lett.* **86**, 787–790. (doi:10.1103/PhysRevLett.86.787)

30. Mailybaev AA, Kirillov ON, Seyranian AP. 2005 Geometric phase around exceptional points. *Phys. Rev. A* **72**, 014104. (doi:10.1103/PhysRevA.72.014104)
31. Berry MV. 1984 Quantal phase factors accompanying adiabatic changes. *Proc. R. Soc. Lond. A* **392**, 45–57. (doi:10.1098/rspa.1984.0023)
32. Latinne O, Kylstra NJ, Dörr M, Purvis J, Terao-Dunseath M, Joachain C, Burke PG, Noble CJ. 1995 Laser-induced degeneracies involving autoionizing states in complex atoms. *Phys. Rev. Lett.* **74**, 46–49. (doi:10.1103/PhysRevLett.74.46)
33. Lee S-Y. 2010 Geometrical phase imprinted on eigenfunctions near an exceptional point. *Phys. Rev. A* **82**, 064101. (doi:10.1103/PhysRevA.82.064101)
34. Nenciu G, Rasche G. 1992 On the adiabatic theorem for nonself-adjoint Hamiltonians. *J. Phys. A: Math. Gen.* **25**, 5741–5751. (doi:10.1088/0305-4470/25/21/027)
35. Graefe E-M, Mailybaev AA, Moiseyev N. 2013 Breakdown of adiabatic transfer of light in waveguides in the presence of absorption. *Phys. Rev. A* **88**, 033842. (doi:10.1103/PhysRevA.88.033842)
36. Milburn TJ, Doppler J, Holmes CA, Portolan S, Rotter S, Rabl P. 2015 General description of quasiadiabatic dynamical phenomena near exceptional points. *Phys. Rev. A* **92**, 052124. (doi:10.1103/PhysRevA.92.052124)
37. Uzdin R, Mailybaev A, Moiseyev N. 2011 On the observability and asymmetry of adiabatic state flips generated by exceptional points. *J. Phys. A Math. Theor.* **44**, 435302. (doi:10.1088/1751-8113/44/43/435302)
38. Gilary I, Mailybaev AA, Moiseyev N. 2013 Time-asymmetric quantum-state-exchange mechanism. *Phys. Rev. A* **88**, 010102. (doi:10.1103/PhysRevA.88.010102)
39. Hassan AU, Zhen B, Soljačić M, Khajavikhan M, Christodoulides DN. 2017 Dynamically encircling exceptional points: exact evolution and polarization state conversion. *Phys. Rev. Lett.* **118**, 093002. (doi:10.1103/PhysRevLett.118.093002)
40. Zhang X-L, Wang S, Hou B, Chan CT. 2018 Dynamically encircling exceptional points: in situ control of encircling loops and the role of the starting point. *Phys. Rev. X* **8**, 021066. (doi:10.1103/PhysRevX.8.021066)
41. Yoon JW *et al.* 2018 Time-asymmetric loop around an exceptional point over the full optical communications band. *Nature* **562**, 86–90. (doi:10.1038/s41586-018-0523-2)
42. Zhang X-L, Jiang T, Chan CT. 2019 Dynamically encircling an exceptional point in anti-parity-time symmetric systems: asymmetric mode switching for symmetry-broken modes. *Light Sci. Appl.* **8**, 88. (doi:10.1038/s41377-019-0200-8)
43. Choi Y, Hahn C, Yoon JW, Song SH, Berini P. 2017 Extremely broadband, on-chip optical nonreciprocity enabled by mimicking nonlinear anti-adiabatic quantum jumps near exceptional points. *Nat. Commun.* **8**, 14154. (doi:10.1038/ncomms14154)
44. Christensen J, Willatzen M, Velasco VR, Lu MH. 2016 Parity-time synthetic phononic media. *Phys. Rev. Lett.* **116**, 207601. (doi:10.1103/PhysRevLett.116.207601)
45. Shi C, Dubois M, Chen Y, Cheng L, Ramezani H, Wang Y, Zhang X. 2016 Accessing the exceptional points of parity-time symmetric acoustics. *Nat. Commun.* **7**, 11110. (doi:10.1038/ncomms11110)
46. Ding K, Ma G, Xiao M, Zhang ZQ, Chan CT. 2016 Emergence, coalescence, and topological properties of multiple exceptional points and their experimental realization. *Phys. Rev. X* **6**, 021007. (doi:10.1103/PhysRevX.6.021007)
47. Ding K, Ma G, Zhang ZQ, Chan CT. 2018 Experimental demonstration of an anisotropic exceptional point. *Phys. Rev. Lett.* **121**, 085702. (doi:10.1103/PhysRevLett.121.085702)
48. Zhao D, Shen Y, Zhang Y, Zhu X, Yi L. 2016 Bound states in one-dimensional acoustic parity-time-symmetric lattices for perfect sensing. *Phys. Lett. A* **380**, 2698–2702. (doi:10.1016/j.physleta.2016.06.022)
49. Shen C, Li J, Peng X, Cummer SA. 2018 Synthetic exceptional points and unidirectional zero reflection in non-Hermitian acoustic systems. *Phys. Rev. Mater.* **2**, 125203. (doi:10.1103/PhysRevMaterials.2.125203)
50. Liu T, Zhu X, Chen F, Liang S, Zhu J. 2018 Unidirectional wave vector manipulation in two-dimensional space with an all passive acoustic parity-time-symmetric metamaterials crystal. *Phys. Rev. Lett.* **120**, 124502. (doi:10.1103/PhysRevLett.120.124502)
51. Zhu W, Fang X, Li D, Sun Y, Li Y, Jing Y, Chen H. 2018 Simultaneous observation of a topological edge state and exceptional point in an open and non-Hermitian acoustic system. *Phys. Rev. Lett.* **121**, 124501. (doi:10.1103/PhysRevLett.121.124501)

52. Achilleos V, Theocharis G, Richoux O, Pagneux V. 2017 Non-Hermitian acoustic metamaterials: role of exceptional points in sound absorption. *Phys. Rev. B* **95**, 144303. (doi:10.1103/PhysRevB.95.144303)
53. Sweeney WR, Hsu CW, Rotter S, Stone AD. 2019 Perfectly absorbing exceptional points and chiral absorbers. *Phys. Rev. Lett.* **122**, 093901. (doi:10.1103/PhysRevLett.122.093901)
54. Nassar H, Chen H, Norris AN, Huang GL. 2017 Non-reciprocal flexural wave propagation in a modulated metabeam. *Extreme Mech. Lett.* **15**, 97–102. (doi:10.1016/j.eml.2017.07.001)
55. Wu Q, Chen Y, Huang G. 2019 Asymmetric scattering of flexural waves in a parity-time symmetric metamaterial beam. *J. Acoust. Soc. Am.* **146**, 850–862. (doi:10.1121/1.5116561)
56. Lustig B, Elbaz G, Muhafra A, Shmuel G. 2019 Anomalous energy transport in laminates with exceptional points. *J. Mech. Phys. Solids* **133**, 103719. (doi:10.1016/j.jmps.2019.103719)
57. Huang J, Zhou X. 2019 A time-varying mass metamaterial for non-reciprocal wave propagation. *Int. J. Solids Struct.* **164**, 25–36. (doi:10.1016/j.ijsolstr.2018.12.029)
58. Huang J, Zhou X. 2020 Non-reciprocal metamaterials with simultaneously time-varying stiffness and mass. *J. Appl. Mech.* **87**, 071003. (doi:10.1115/1.4046844)
59. Ma F, Imam A, Morzfeld M. 2009 The decoupling of damped linear systems in oscillatory free vibration. *J. Sound Vibr.* **324**, 408–428. (doi:10.1016/j.jsv.2009.02.005)
60. Veletsos AS, Ventura CE. 1986 Modal analysis of non-classically damped linear systems. *Earthquake Engng Struct Dyn.* **14**, 217–243. (doi:10.1002/eqe.4290140205)